NJC

ROYAL SOCIETY OF CHEMISTRY

PAPER

View Article Online
View Journal | View Issue

Cite this: *New J. Chem.*, 2022, **46**, 20146

ZnCdS enhanced g-C_3N_4 electrochemiluminescence behavior based on $Rh_{0.6}Ru_{0.4}$@Ag quenching for neuron-specific enolase detection†

Zhengxing Gong,[ab] Jing Luo,[ab] Xinrong Shao,[ab] Xu Sun,[ab] Huan Wang,[ab] Dan Wu,[ab] Dawei Fan,*[ab] Yuyang Li,[ab] Qin Wei[ab] and Huangxian Ju[abc]

Received 29th August 2022,
Accepted 26th September 2022

DOI: 10.1039/d2nj04308d

rsc.li/njc

A novel quenching electrochemiluminescence (ECL) immunosensor for the trace detection of neuron-specific enolase (NSE) was developed. Doping CdS with Zn^{2+} to obtain ZnCdS not only significantly improves the original properties of CdS, but also can be loaded onto the surface of g-C_3N_4 to form a special complex structure, which effectively improves the ECL performance of g-C_3N_4. $Rh_{0.6}Ru_{0.4}$ alloys with flower-like structures were prepared by simple hydrothermal synthesis, with excellent electrical conductivity and catalytic performance. Due to its special flower-like structure with a large specific surface area, Ag nanoparticles can be uniformly loaded on its surface to form $Rh_{0.6}Ru_{0.4}$@Ag composites. Through spectral comparison, it was found that $Rh_{0.6}Ru_{0.4}$@Ag has strong UV-vis absorption in the ECL emission wavelength range of g-C_3N_4, which can generate resonance energy transfer, thereby effectively quenching the ECL signal. The immunosensor has a wide detection range with a detection limit of 16 fg mL^{-1} (S/N = 3), good stability and biocompatibility, and has great potential in clinical application.

1. Introduction

Small cell carcinoma (SCLC) has the characteristics of easy metastasis, rapid proliferation, high malignant degree, poor prognosis and no obvious clinical symptoms in the early stage.[1–4] Most patients with SCLC have developed to the middle and late stages when they are diagnosed, and even if they are treated, the survival rate of patients is low.[5,6] Therefore, it is of great significance to diagnose SCLC early. As a tumor marker, neuron-specific enolase (NSE) is a brain protein located in neuroendocrine cells, with high specificity and sensitivity, and its content can be used as a standard to distinguish normal people from patients.[7,8] Although many analytical methods for detecting NSE have been developed, most of these methods require complicated procedures, expensive instruments and high expenditure.[9,10] Therefore, the development of a more convenient and accurate method for detecting NSE has become the main research direction.[11]

g-C_3N_4 is a semiconductor material with a two-dimensional structure composed of a π conjugated graphite plane, which has a suitable energy band structure and physical and chemical properties, including good thermal stability, excellent chemical stability and excellent photoelectric properties.[12–14] It is well known that g-C_3N_4 can form hetero-structures with a series of substances, and accelerate electron transfer. Zn^{2+} doping of CdS can improve the surface properties and band gap of the semiconductor, and form a complex structure with g-C_3N_4 to stabilize its luminescence performance.[15]

Electrochemiluminescence (ECL) is a multifunctional analytical technique that converts electric energy into light energy.[16–18] The excited state of the substances produced on the electrode surface is formed by electron transfer, which is a special chemiluminescence phenomenon on the electrode.[19,20] Therefore, it is an ideal combination of electrochemistry and spectroscopy, and it has been widely used in diagnosis, analysis and environmental detection for its unique performance.[21–24] Generally speaking, the presence of co-reactants will greatly improve the signal and stability of the luminophore, such as

[a] *Collaborative Innovation Center for Green Chemical Manufacturing and Accurate Detection, School of Chemistry and Chemical Engineering, University of Jinan, Jinan 250022, People's Republic of China. E-mail: jndxfandawei@126.com; Tel: +86-531-82760510*

[b] *Key Laboratory of Interfacial Reaction & Sensing Analysis in Universities of Shandong, School of Chemistry and Chemical Engineering, University of Jinan, Jinan 250022, People's Republic of China*

[c] *State Key Laboratory of Analytical Chemistry for Life Science, School of Chemistry and Chemical Engineering, Nanjing University, Nanjing 210023, People's Republic of China*

† Electronic supplementary information (ESI) available. See DOI: https://doi.org/10.1039/d2nj04308d

tertiary amine as the co-reactant of $Ru(bpy)_3^{2+}$ and $S_2O_8^{2-}$ as the reactant of quantum dots.[25–27] CdS, a widely studied semiconductor material, has become a hot topic due to its excellent performance.[28,29] However, research shows that CdS still has defects, and Zn^{2+} doping can improve the surface properties and band gap of semiconductor CdS.[30] The doped new product ZnCdS and g-C_3N_4 form a complex structure, which enhances and stabilizes the luminescence of g-C_3N_4.

In this paper, a sandwich-type quenching electrochemiluminescence immunosensor has been successfully prepared, which can sensitively detect NSE. First, ZnCdS nanoparticles (NPs) were synthesized and fixed on g-C_3N_4 nanosheets to form a complex structure, which stabilized the luminescent properties of g-C_3N_4. With Ag NPs, $Rh_{0.6}Ru_{0.4}$ has stronger conductivity, and improves the performance of the sensor. The ECL signal of g-C_3N_4 can be weakened by resonance energy transfer because the UV-vis spectrum of $Rh_{0.6}Ru_{0.4}$@Ag overlaps with the ECL emission spectrum of g-C_3N_4 in a large range. At the same time, the sensitivity of the sensor can be improved. Finally, it is found that the prepared sensor has good sensitivity, which provides a feasible method for NSE detection.

2. Experimental

2.1. Reagents

Neuron-specific enolase (NSE), neuron-specific enolase capture antibody (Ab_1), detection antibody (Ab_2), carcinoembryonic antigen (CEA), alpha fetoprotein (AFP), glucose (Glu), procalcitonin (PCT), aflatoxin (AFT) and insulin (Ins) were all brought from Shanghai Linc-Bio Science Co. Ltd (Shanghai, China). Melamine, chromium nitrate tetrahydrate ($Cd(NO_3)_2$ $4H_2O$),

Zhengxing Gong is a master's student in the school of chemistry and chemical engineering, University of Jinan. His current research interests are electrochemiluminescence sensors and nanomaterials.

Jing Luo is a master's student in the school of chemistry and chemical engineering, University of Jinan. Her current research interests are photoelectrochemical sensors and nanomaterials.

Xinrong Shao is a master's student in the school of chemistry and chemical engineering, University of Jinan. Her current research interests are electrochemiluminescence sensors and nanomaterials.

Xu Sun received her PhD in inorganic chemistry at the University of Science and Technology of China (USTC). She is now working as an associate professor in the School of Chemistry and Chemical Engineering, University of Jinan. Her research interests focus on the design and fabrication of novel nanomaterials for the construction of energy-related devices.

Huan Wang received his PhD degree in China University of Geosciences (Beijing) in 2017. Now, he is engaged in teaching and scientific research in the School of Chemistry and Chemical Engineering, Jinan University. His current research interests are nanometer material preparation, electrochemical biosensors, photoelectric materials and applications.

Dan Wu received her DS degree from Shandong University in 2005. Her studies are focused on the surfactant and biological macromolecule interaction. And now she also studies the role of surfactant in electrochemical immunosensors.

Dawei Fan received her PhD degree from Lanzhou institute of chemical physics, Chinese academy of sciences. Now, she is an associate professor at the University of Jinan. Her main research interests are electrochemical sensors and photoelectrochemical sensors. She has published over 50 articles on analysis and immunosensor and applied successfully for many research projects, such as Angewandte Chemie International Edition, Biosensors & Bioelectronics, Journal of Physical Chemistry C, and ACS Applied Materials & Interfaces.

Yuyang Li received his PhD degree from China University of Petroleum (East China) in 2018. His main research interests are the design and preparation of functional nano-material, sensor technology, fluorescence imaging, and their industrial application. He has been hosting one national scientific research project.

Qin Wei, a professor and DSc, has devoted herself to analytical teaching and scientific research. Her main research interests are the determination of protein and nucleic acid by photometry and the electrochemical immunosensor preparation. She has published over two hundred articles on analysis and immunosensor and applied successfully for many research projects, such as Analytical Chemistry, Advanced Functional Materials, Chemical Communication, Biosensors & Bioelectronics, Journal of Materials Chemistry A, and ACS Applied Materials & Interfaces.

Huangxian Ju received his BS, MS and PhD degrees from Nanjing University during the period 1982–1992. He was a postdoc in Montreal University (Canada) in 1996–1997. He became an associate and full professor of Nanjing University in 1993 and 1999. He is currently the director of State Key Laboratory of Analytical Chemistry for Life Sciences. His research interests focus on analytical biochemistry, biosensing and molecular diagnosis. He has published 690 papers in different journals with h-index of 91 (Google Scholar h-index 100 with 35298 citations).

sodium sulfide nonahydrate ($Na_2S{\cdot}9H_2O$), zinc acetate dihydrate ($Zn(Ac)_2{\cdot}2H_2O$), bovine serum albumin (BSA, 96–98%), silver nitrate ($AgNO_3$), rhodium acetylacetone, and ruthenium acetylacetone were acquired from Macklin Industrial Corporation. Ethanol and sodium citrate were supplied by Sinopharm Chemical. N-hydroxysuccinimide (NHS), 1-(3-dimethylaminopropyl)-3-ethylcarbodiimide hydrochloride (EDC), KH_2PO_4, Na_2HPO_4 and luminol were obtained from Aladdin (Shanghai China).

2.2. Preparation of $Rh_{0.6}Ru_{0.4}$@Ag-Ab_2

According to a previous report,[31] typically, 6 mg of $Rh(acac)_3$ and 3 mg of $Ru(acac)_3$ were dissolved in 8 mL of water. After ultrasonic dispersion, 1 mL of formaldehyde solution was added dropwise under magnetic stirring. Under continuous stirring, the solution changed color. Finally, the precursor liquid was transferred to Teflon-lined stainless-steel autoclave with a capacity of 20 mL, and maintain at 180 °C for 7 h.

The following steps are used to synthesize $Rh_{0.6}Ru_{0.4}$@Ag-Ab_2. First of all, the prepared $Rh_{0.6}Ru_{0.4}$ and Ag NPs were shaken for 8 h to prepare $Rh_{0.6}Ru_{0.4}$@Ag. 1 mg of $Rh_{0.6}Ru_{0.4}$@Ag was uniformly dispersed in 2 mL PBS (phosphate buffered saline); then 1 mL Ab_2 (1 μg mL^{-1}) was added and shaken at 4 °C. Next, to occupy the nonspecific site, 500 μL BSA (1 wt%) was added and incubated at 4 °C for 6 h.

2.3. Fabrication procedure of the ECL immunosensor

First, in order to obtain a glassy carbon electrode (GCE) with a smooth mirror surface, 0.05 micron alumina powder was used for polishing and ultrapure water was used for cleaning. 10 μL g-C_3N_4/ZnCdS (3 mg mL^{-1}) was dropped on the surface of a well-polished GCE and dried at room temperature. Then 6 μL EDC-NHS (1 mg mL^{-1}) solution was dripped on the electrode to activate the carboxyl groups. Following this, the electrode was covered with 6 μL Ab_1 (1 μg mL^{-1}) solution in sequence and stored at 4 °C until dry. To block nonspecific binding sites, 3 μL of BSA (1 wt%) solution was inoculated on the electrode surface for 1 h. Then different concentrations of NSE were modified and dried at 4 °C. Finally, 5 μL $Rh_{0.6}Ru_{0.4}$@Ag-Ab_2 (1 mg mL^{-1}) solution was used to modify the electrode surface (Scheme 1). After each step, the electrode surface was cleaned with PBS (pH 7.4).

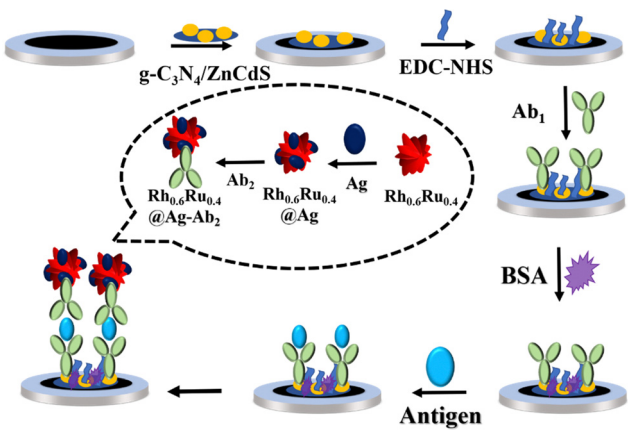

Scheme 1 Construction process of the quenching ECL immunosensor. Illustration shows the preparation step of $Rh_{0.6}Ru_{0.4}$@Ag-Ab_2.

3. Results and discussion

3.1. Material characterization

The synthesized g-C_3N_4 has a nano-sheet structure with a large surface area (Fig. 1A), which makes it possible to load ZnCdS. The peaks of XRD shown in Fig. 1E prove the successful synthesis of g-C_3N_4.[32] ZnCdS consists of relatively uniform and easy-to-agglomerate nanoparticles (Fig. S1, ESI†), and the particle size analysis shows that the size is mostly 7.5 nm (Fig. S2, ESI†). The smaller size can make a large amount of ZnCdS adhere to g-C_3N_4, thus enhancing the conductivity of g-C_3N_4. From the HRTEM image of ZnCdS shown in Fig. 1B, it can be seen that its l lattice fringes is measured at d = 0.332 nm,[33] which further proves that the synthesis of ZnCdS is successful. Fig. 1D shows that there are many characteristic peaks in the XRD spectrum of ZnCdS, such as 25.5°, 27.0°, 28.6°, 44.3°, 48.3° and 52.4°, which, respectively, correspond to (100), (002), (101), (110), (103) and (112) in the standard XRD spectrum (PDF#89-2943).[34] By comparing Fig. 1A with Fig. 1C, it can be found that a large number of nanoparticles are attached to the nanosheets of the original g-C_3N_4 thin layer, which indicates that g-C_3N_4 and ZnCdS successfully compound into heterostructures.

As shown in Fig. 2A, the prepared $Rh_{0.6}Ru_{0.4}$ has a flower-like structure formed by the overlapping of many nano-sheets. Due to the large specific surface area, more Ag NPs can be loaded, and the conductivity of the composite is improved. In the synthesis method, the ratio of Ru and Rh elements in the alloy is controlled by controlling the contents of $Rh(acac)_3$ and $Ru(acac)_3$ terpyridine. It can be seen from the element content analysis in Fig. 2B that the element ratio in the alloy combines the expected effect and the EDS element mapping images of Ru and Rh (Fig. 2C and D) clearly show the uniform distribution and high overlap of elements.

3.2. ECL behavior of g-C_3N_4/ZnCdS

As can be seen from Fig. 3A, compared with the bare glassy carbon electrode, g-C_3N_4 shows a good ECL signal. Compared with curve (b), the ECL signal of g-C_3N_4 in curve (c) is further enhanced at the same concentration. The results show that the complex structure of ZnCdS and g-C_3N_4 can promote the ECL reaction.

The possible ECL mechanism of the signal immunosensor is as follows. When a negative voltage is applied, on the electrode surface, g-C_3N_4 acquires electrons (eqn (1)) and becomes g-$C_3N_4^{\bullet-}$. The $S_2O_8^{2-}$ gets electrons to generate $SO_4^{\bullet-}$ and SO_4^{2-} at the same time (eqn (2)). $SO_4^{\bullet-}$ will react with g-$C_3N_4^{\bullet-}$ to produce excited g-C_3N_4* (eqn (4)). Finally, when g-C_3N_4* becomes g-C_3N_4 (eqn (5)), it will be accompanied by the generation of light and the light will be detected by the instrument. The existence of ZnCdS will catalyze the generation of $SO_4^{\bullet-}$ (eqn (3)), produce more excited g-C_3N_4*, and enhance the luminescence signal.

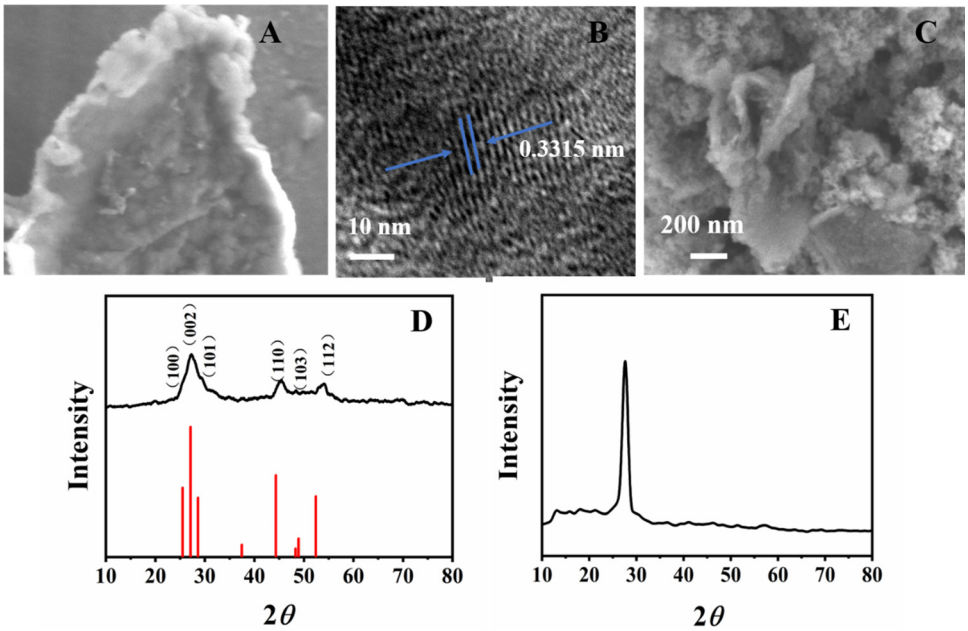

Fig. 1 SEM images of (A) g-C_3N_4 and (C) g-C_3N_4/ZnCdS. HRTEM images of (B) ZnCdS. XRD patterns of (D) ZnCdS and (E) g-C_3N_4.

After the quenching agent $Rh_{0.6}Ru_{0.4}$@Ag was added, the ECL signal of the sensor decreased obviously (Fig. 3A(b)), so the quenching principle of the sensor was explored. The ECL emission spectrum of g-C_3N_4/ZnCdS and the UV-vis absorption spectrum of $Rh_{0.6}Ru_{0.4}$@Ag were analyzed. And the light emitted by g-C_3N_4/ZnCdS (Fig. 3B(a)) on the surface of the electrode is 420–800 nm, and the intensity of the light is the highest at 470 nm. Compared with g-C_3N_4, the peak shifted to the right by 10 nm,[35] which once again showed that ZnCdS was successfully combined with g-C_3N_4. The UV-vis absorption of $Rh_{0.6}Ru_{0.4}$@Ag overlaps with the ECL emission spectrum of g-C_3N_4/ZnCdS which indicates that the ECL signal is effectively quenched by resonance energy transfer.[36]

Eqn (1)–(5).

$$\text{g-}C_3N_4 + e^- \rightarrow \text{g-}C_3N_4^{\bullet -} \quad (1)$$

$$S_2O_8^{2-} + e^- \rightarrow SO_4^{2-} + SO_4^{\bullet -} \quad (2)$$

$$S_2O_8^{2-} + e^- \xrightarrow{\text{ZnCdS}} SO_4^{2-} + SO_4^{\bullet -} \text{ (more)} \quad (3)$$

$$\text{g-}C_3N_4^{\bullet -} + SO_4^{\bullet -} \rightarrow \text{g-}C_3N_4^{*} + SO_4^{2-} \quad (4)$$

$$\text{g-}C_3N_4^{*} \rightarrow \text{g-}C_3N_4 + h\nu \quad (5)$$

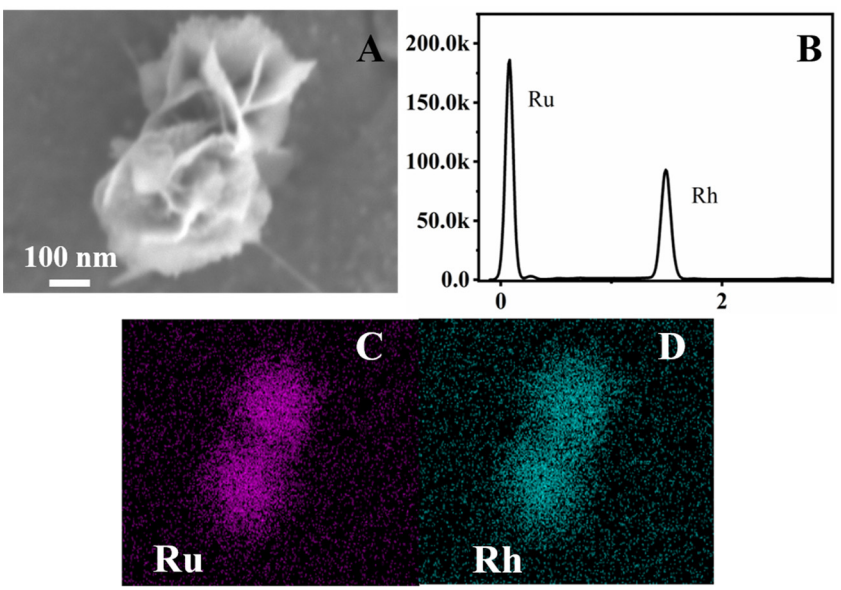

Fig. 2 (A) SEM of images of $Rh_{0.6}Ru_{0.4}$ and EDS element mapping images of Ru (C) and Rh (D). (B) EDX spectra of $Rh_{0.6}Ru_{0.4}$.

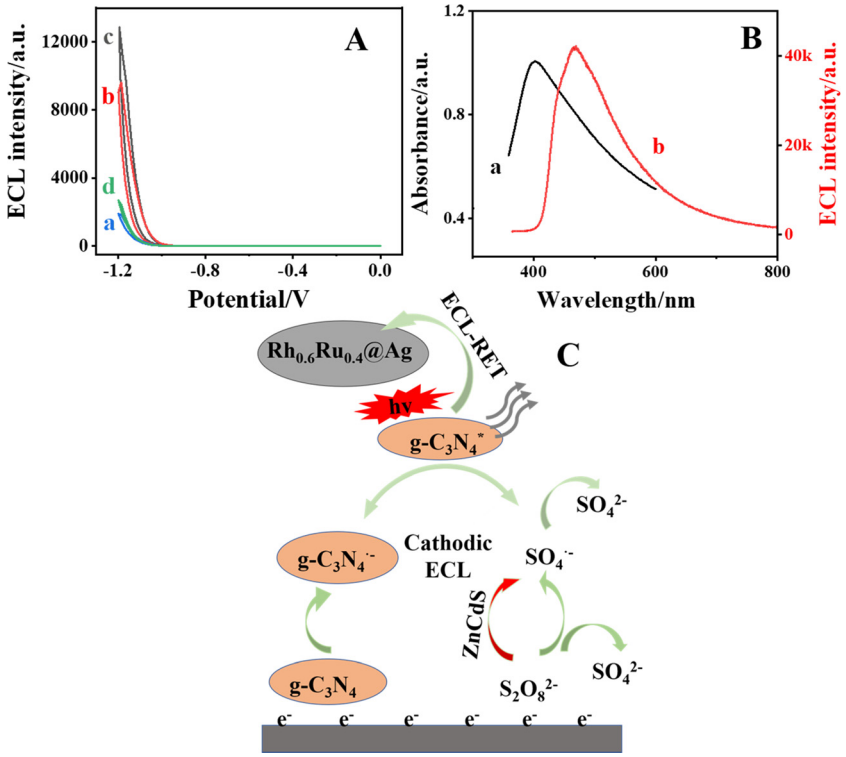

Fig. 3 (A) ECL responses of (curve a) bare GCE, (curve b) g-C_3N_4/GCE, (curve c) g-C_3N_4/ZnCdS/GCE, and (curve d) $Rh_{0.6}Ru_{0.4}$@Ag-Ab_2/Ag/BSA/Ab_1/g-C_3N_4/ZnCdS/GCE in 10 mL PBS (pH 7.4) with 100 mM $K_2S_2O_8$. (B) UV-vis absorption diagram of $Rh_{0.6}Ru_{0.4}$ (curve a) and ECL emission diagram of g-C_3N_4/ZnCdS (curve b). ECL process in a system without (C).

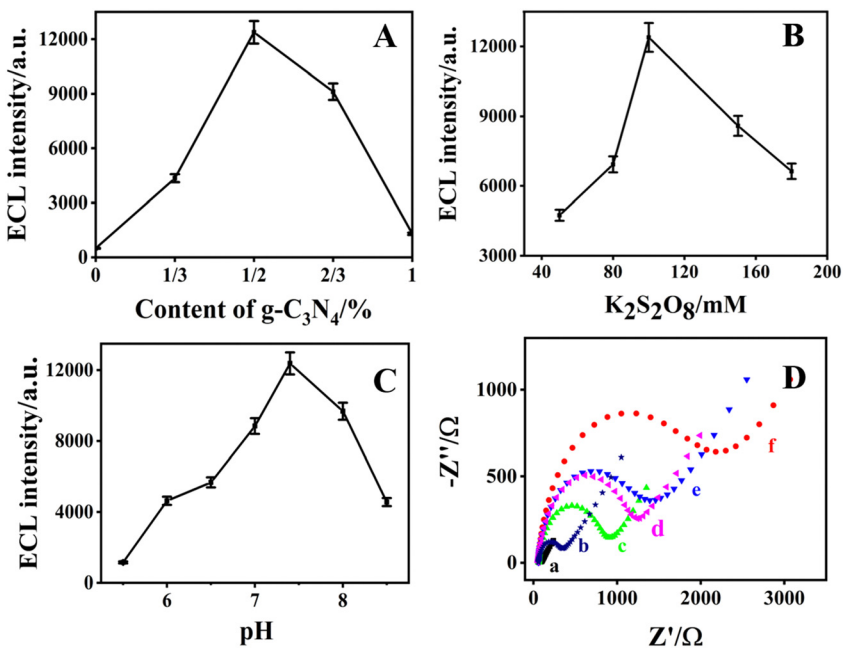

Fig. 4 (A) The mass of g-C_3N_4 in the compound. Dependence of ECL responses on (B) $K_2S_2O_8$, (C) pH value; all ECL test voltages are −1.6 to 0 V. (D) EIS of (curve a) bare GCE, (curve b) g-C_3N_4/ZnCdS/GCE, (curve c) Ab_1/g-C_3N_4/ZnCdS/GCE, (curve d) BSA/Ab_1/g-C_3N_4/ZnCdS/GCE, (curve e) Ag/BSA/Ab_1/g-C_3N_4/ZnCdS/ZnCdS/GCE, and (curve f) $Rh_{0.6}Ru_{0.4}$@Ag-Ab_2/Ag/BSA/Ab_1/g-C_3N_4/ZnCdS/GCE. The error bars show the standard deviation of quintuplicate tests (N = 5).

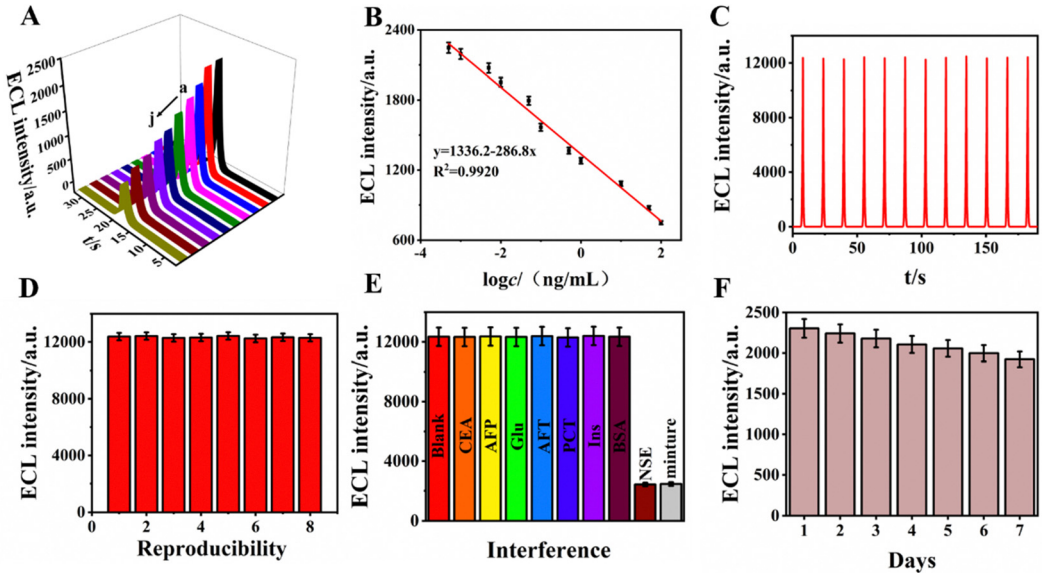

Fig. 5 (A) The ECL intensity–time curves of different concentrations of NSE detected by the immunosensor: (a) 0.00005, (b) 0.0001, (c) 0.0005, (d) 0.005, (e) 0.01, (f) 0.1, (g) 1, (h) 10, (i) 50, and (j) 100 ng mL^{-1}. (B) Calibration curve of the immunosensor. (C) Stability of immunosensor under continuous scanning. (D) Repeatability of the immunosensor of different electrodes. (F) Selectivity of immunosensors prepared: blank, CFA, AFP, Glu, AFT, PCT, Ins, BSA, AFP, NSE, and mixture. The error bars show the standard deviation of quintuplicate tests (N = 5).

3.3. Optimization of the experimental conditions

First, the ratio of g-C_3N_4 to ZnCdS was investigated. When the mass of g-C_3N_4 accounts for 50% of the mass of the composite, the signal generated is the strongest (Fig. 4A). The pH can seriously affect the behaviour of the immunosensor. For this reason, the signal of the immunosensor is detected at different pH values. It can be seen from Fig. 4B that when the pH value is between 6.5 and 7.4, the signal of the immunosensor gradually increases, and when the pH value exceeds 7.4, the signal begins to weaken. So the optimal pH value of the immunosensor is 7.4. At the same time, the concentration of the co-reactant, potassium persulfate, was optimized. With the increase of potassium persulfate concentration, the signal of the immunosensor increases until the concentration of potassium persulfate is 100 mM, then the signal begins to decrease. Therefore, the optimal concentration is 100 mM (Fig. 4C).

3.4. EIS characterization of the immunosensor

In order to verify whether the immunosensor was successfully built, EIS test was carried out. From Fig. 4D it can be observed that the impedance of the bare glassy carbon electrode is very small. The impedance of the electrode increases due to the modification of g-C_3N_4/ZnCdS on the surface of the electrode, but it still has good conductivity. With the modification of BSA, Ab_1 and Agent biomolecules, the electrode resistance gradually increases, which illustrates the successful bonding on the electrode surface. When the last layer is modified (Fig. 4D(f)), the impedance does not change much, which indicates that $Rh_{0.6}Ru_{0.4}$@Ag has good conductivity.

3.5. ECL detection of the fabricated immunosensor

Under the best experimental conditions, NSE was detected by the immunosensor. It can be seen from Fig. 5A that the ECL intensity shows a downward trend with the increase of NSE concentration. When the concentration range is 0.5 pg mL^{-1}–100 ng mL^{-1}, the linear formula of log c and ECL intensity is I = 1336.2–286.8 lg c, the correlation coefficient is 0.992 (Fig. 5B), and the detection limit is 16 fg mL^{-1}.

3.6. Stability, selectivity and reproducibility of the ECL response

In clinical medical detection, immunosensors have higher requirements for stability and selectivity. Under the best experimental conditions, the immunosensor has been scanned continuously for 12 cycles. Fig. 5C shows the ECL signal is very stable, and the calculated relative deviation is 3.8%, which has good stability. Fig. 5D shows that the ECL signals of the immunosensor are reproducible; the relative standard deviation

Table 1 Performance comparison with other documents

Methods	Detection range (ng mL^{-1})	Detection limit (pg mL^{-1})	Ref.
Photoelectrochemical interface	0.00001–1000	0.043	37
Electrochemical	0.5–100	0.0257	38
Microfluidic paper-based analytical devices	1–500	10	39
Surface plasmon resonance	10–100	500	40
Electrochemiluminescence	0.00005–100	0.016	This work

is 2.1%, certifying that the immunosensor has good reproducibility. After storing the electrode for 7 days and measuring its ECL signal every day, it was found that the signal of the electrode drops by 16% after 7 days.

In order to evaluate the sensitivity and selectivity of the immunosensor, carcinoembryonic antigen (CEA), alpha-fetoprotein (AFP), glucose (Glu), aflatoxin (AFT), calcitonin (PCT), insulin (Ins), bovine serum albumin (BSA) and their mixture were used as the interfering substances, at the concentration of 10 ng mL^{-1}. As shown in Fig. 5E, the ECL signals of the interfering substance are almost the same as that of the bare electrode. When the interfering substance and NSE exist at the same time, the ECL signal changes obviously, which indicates that the immunosensor has good selectivity (Table 1).

4. Conclusions

In this paper, a quenching sandwich-type immunosensor was constructed to detect NSE. ZnCdS, a semiconductor nanomaterial with good performance, was successfully synthesized by doping CdS with Zn^{2+}. After forming a complex structure with g-C_3N_4, the ECL spectrum of g-C_3N_4 is shifted, and the ECL luminescent properties of g-C_3N_4 are stabilized. $Rh_{0.6}Ru_{0.4}$ was synthesized by a simple hydrothermal method, and Ag was modified on its surface as a capture antibody marker. When g-C_3N_4 was incubated with $Rh_{0.6}Ru_{0.4}$@Ag-Ab_2, the ECL signal of g-C_3N_4 was decreased due to resonance energy transfer. Owing to its good stability, high sensitivity and excellent selectivity, the immunosensor can detect low concentration of NSE.

Conflicts of interest

There are no conflicts to declare.

Acknowledgements

This research was financially supported by the Innovation Team Project of Colleges and Universities in Jinan (No. 2019GXRC027), and the National Natural Science Foundation of China (No. 51904114, 21777056, 21675063), the Special Foundation for Taishan Scholar Professorship of Shandong Province.

References

1 C. Karaman, O. S. Bolükbas, B. B. Yola, O. Karaman, N. Atar and mL. Yola, *Anal. Chim. Acta*, 2022, **1200**, 339609.
2 V. Longo, A. Catino, M. Montrone, P. Pizzutilo, T. Annese, F. Pesola, I. Marech, S. Cassiano, D. Ribatti and D. Galetta, *Int. J. Mol. Sci.*, 2021, **22**, 11123.
3 C. Crockett, J. Belderbos, A. Levy, F. McDonald, L. C. Pechoux and C. Faivre-Finn, *Lung Cancer*, 2021, **162**, 96–105.
4 L. Niu, L. Chen, Y. Li, Z. Hu and F. He, *Semin. Cancer Biol.*, 2022, DOI: **10.1016/j.semcancer.2022.03.009**.
5 U. Tapan, V. F. Furtado, M. M. Qureshi, P. Everett, K. Suzuki and K. S. Mak, *JTO Clin. Res. Rep.*, 2021, **2**, 100109.
6 M. K. Baine, M. S. Hsieh, W. V. Lai, J. V. Egger, A. A. Jungbluth, Y. Daneshbod, A. Beras, R. Spencer, J. Lopardo, F. Bodd, J. Montecalvo, J. L. Sauter, J. C. Chang, D. J. Buonocore, W. D. Travis, T. Sen, J. T. Poirier, C. M. Rudin and N. Rekhtman, *J. Thorac. Oncol.*, 2020, **15**, 1823–1835.
7 C. M. Rudin, E. Brambilla, C. Faivre-Finn and J. Sage, *Nat. Rev. Dis. Primers*, 2021, **7**, 3.
8 Y. Chen, X.-Y. Ge, S.-Y. Cen, A.-J. Wang, X. Luo and J.-J. Feng, *Sens. Actuators, B*, 2020, **311**, 127931.
9 M. G. Raso, N. Bota-Rabassedas and I. I. Wistuba, *Cancers*, 2021, **13**, 820.
10 A. Muraleedharan, S. U. Velladath and B. VS, *Diabetes Metab. Syndr.*, 2020, **14**, 1061–1063.
11 C. Xu, Y. Luo, S. Li, Z. Li, L. Jiang, G. Zhang, L. Owusu and H. L. Chen, *Biosci. Rep.*, 2019, **39**, BSR20192732.
12 J. Fu, J. Yu, C. Jiang and B. Cheng, *Adv. Energy Mater.*, 2018, **8**, 1701503.
13 M. B. Shekardasht, M. H. Givianrad, P. Gharbani, Z. Mirjafary and A. Mehrizad, *Diamond Relat. Mater.*, 2020, **109**, 108008.
14 Z. Yang, X. Wu, X. Liu and M. Xu, *Chin. J. Anal. Chem.*, 2021, **49**, e21179–e21186.
15 N. Zhang, C. Chen, Y. Chen, G. Chen, C. Liao, B. Liang, J. Zhang, A. Li, B. Yang, Z. Zheng, X. Liu, A. Pan, S. Liang and R. Ma, *ACS Appl. Energy Mater.*, 2018, **1**, 2016–2023.
16 L. Hu and G. Xu, *Chem. Soc. Rev.*, 2010, **39**, 3275–3304.
17 H. Qi, Y. Peng, Q. Gao and C. Zhang, *Sensors*, 2009, **9**, 674–695.
18 X. Shao, X. Song, X. Liu, L. Yan, L. Liu, D. Fan, Q. Wei and H. Ju, *Mikrochim. Acta*, 2021, **188**, 344.
19 S. Kulmala and J. Suomi, *Anal. Chim. Acta*, 2003, **500**, 21–69.
20 C. K. P. Truong, T. D. D. Nguyen and I.-S. Shin, *BioChip J.*, 2019, **13**, 203–216.
21 X. Zhou, W. Zhang, Z. Wang, J. Han, G. Xie and S. Chen, *Biosens. Bioelectron.*, 2020, **148**, 111795.
22 K. Zhang, Z. Fan, Y. Ding and M. Xie, *Chem. Eng. J.*, 2022, **429**, 132472.
23 X. Zhang, Y. Nie, Q. Zhang, Z. Liang, P. Wang and Q. Ma, *Chem. Eng. J.*, 2021, **411**, 128428.
24 L.-Y. Huang, X. Hu, H.-Y. Shan, L. Yu, Y.-X. Gu, A.-J. Wang, D. Shan, P.-X. Yuan and J.-J. Feng, *Sens. Actuators, B*, 2021, **344**, 130300.
25 A. Jimenez-Ruiz, E. Grueso, P. Perez-Tejeda, F. Muriel-Delgado and C. Torres-Marquez, *Anal. Bioanal. Chem.*, 2016, **408**, 7213–7224.
26 L. Zheng, B. Wang, Y. Chi, S. Song, C. Fan and G. Chen, *Dalton Trans.*, 2012, **41**, 1630–1634.
27 S. Kirschbaum-Harriman, A. Duerkop and A. J. Baeumner, *Analyst*, 2017, **142**, 2648–2653.
28 Y. Chen, W. Zhong, F. Chen, P. Wang, J. Fan and H. Yu, *J. Mater. Sci. Technol.*, 2022, **121**, 19–27.
29 L. Feng, L. Zhang, X. Chen, C. Zhang, G. Mao and H. Wang, *Chem. Eng. J.*, 2022, **441**, 136073.
30 K. Wang, Q. Liu, Q. M. Guan, J. Wu, H. N. Li and J. J. Yan, *Biosens. Bioelectron.*, 2011, **26**, 2252–2257.
31 L. Zhao, X. Liu, S. Zhang, J. Zhao, X. Xu, Y. Du, X. Sun, N. Zhang, Y. Zhang, X. Ren and Q. Wei, *J. Mater. Chem. A*, 2021, **9**, 259–263.
32 X. Li, X. Zhang, H. Ma, D. Wu, Y. Zhang, B. Du and Q. Wei, *Biosens. Bioelectron.*, 2014, **55**, 330–336.

33 W. Zhu, C. Wang, X. Li, M. S. Khan, X. Sun, H. Ma, D. Fan and Q. Wei, *Biosens. Bioelectron.*, 2017, **97**, 115–121.
34 Z. Jiang, Y. Lei, M. Zhang, Z. Zhang and Z. Ouyang, *J. Nanomater.*, 2019, **2019**, 9.
35 C. Zhou, Y. Chen, P. Shang and Y. Chi, *Analyst*, 2016, **141**, 3379–3388.
36 Y. Chu, T. Han, A. Deng, L. Li and J.-J. Zhu, *TrAC, Trends Anal. Chem.*, 2020, **123**, 115745.
37 R. Xu, K. Xu, Y. Du, J. Li, L. Dai, T. Wu, X. Ren and Q. Wei, *Sens. Actuators, B*, 2022, **361**, 131702.
38 X. Yu, Y. Li, Y. Li, S. Liu, Z. Wu, H. Dong, Z. Xu, X. Li and Q. Liu, *Talanta*, 2022, **236**, 122865.
39 Y. Fan, J. Liu, Y. Wang, J. Luo, H. Xu, S. Xu and X. Cai, *Biosens. Bioelectron.*, 2017, **95**, 60–66.
40 M. Toma, S. Izumi and K. Tawa, *Analyst*, 2018, **143**, 858–864.